

Monte Carlo evaluation of the influence of the interaction cross sections on the secondary-electron-emission yields from polycrystalline aluminum targets

A. Dubus and J.-C. Dehaes

*Université Libre de Bruxelles, Service de Métrologie Nucléaire (Code Postal 165),
50, avenue F. D Roosevelt, B-1050, Brussels, Belgium*

J.-P. Ganachaud and A. Hafni

*Université de Nantes, Faculté des Sciences et des Techniques, Laboratoire de Physique du Solide Théorique,
2, rue de la Houssinière, 44072 Nantes CEDEX 03, France*

M. Cailler

*Université de Nantes, Institut des Sciences de l'Ingénieur en Thermique, Energétique et Matériaux (ISITEM),
Laboratoire de Sciences des Surfaces et Interfaces en Mécanique, La Chantrerie (CP3023), 44087 Nantes CEDEX 03, France*

(Received 11 March 1992)

The aim of this paper is to show that different assumptions for the interaction cross sections of low-energy electrons in polycrystalline aluminum targets lead to very different calculated values of secondary-electron yields, either in backscattering or in transmission. We emphasize the importance of the description of elastic collisions, of the choice of the dielectric function, and the role of ionizing collisions. We indicate that the comparisons between the published theoretical results are somewhat intricate due to the differences in the transport description and in the choice of cross sections.

I. INTRODUCTION

Secondary-electron emission (SEE) has been the subject of many experimental and theoretical works. Some recent reviews describe the theoretical aspects of SEE.¹⁻⁷ In most cases, the electron emission is treated as a three-step process. The primary particles (electrons or ions), penetrating into the material, interact elastically and inelastically with the electrons and the ionic cores of the target. The inelastic interactions give rise to excitations of electrons [the internal secondary electrons (SE's)] which undergo elastic and inelastic scatterings. The cascade of inelastic scatterings leads to a multiplication of excited electrons. All the electrons propagate in the solid and some of them, arriving at the surface, can escape through the vacuum-medium potential barrier.

In the literature, many different assumptions are made to treat the electron interactions in solids and their transport in the target. We present here a comparison of Monte Carlo simulation results obtained using various sets of electron interaction cross sections in polycrystalline Al targets. This study is not a critical review giving the best cross sections to choose, but instead an analysis of the sensitivity of the SEE properties to these choices.

We first discuss the SEE models used by several groups. Then we describe the interaction cross sections they have used. Finally, we present some results for polycrystalline Al targets both for backscattering and for transmission geometries. We will limit ourselves in this paper to the calculation of yield values. For the backscattering geometry, we study the true secondary yield δ (defined as the number of electrons, per incident electron, going out with an energy less than 50 eV) and the backscattering yield η (number of electrons going out with an

energy larger than 50 eV) as a function of the incident-electron energy. For the transmission geometry, we study the backscattering and transmission coefficients η_R and η_T (defined as the numbers of electrons going out with an energy larger than 50 eV in the backward and forward directions, respectively) as a function of the target thickness, for 1-keV incident electrons. We emphasize the important role played by the elastic process, compare several dielectric functions for the electron interactions in the jellium, and point out the influence of the ionizing collisions.

II. OVERVIEW OF THE MOST IMPORTANT MICROSCOPIC MODELS OF SECONDARY-ELECTRON EMISSION

Realistic descriptions of SEE were given in the 1950s by Bruining,⁸ Baroody,⁹ Wolff,¹⁰ Sternglass,¹¹ Streitwolf,¹² and Stolz¹³ among others. Their models had the general advantage to be fully analytical models, but for this reason, they had also to use rather rough approximations. Since 1970, more realistic microscopic models have been proposed. In the papers of Bennett and Roth,¹⁴ Chung and Everhart,¹⁵ and in the extensive work made by the groups of Nantes, Osaka, Nice, Berlin, and Brussels, many different assumptions have been used both for the electron interactions and for the transport process. We give below a brief overview of these assumptions.

A very interesting model has been developed by Schou^{2,16} based on an analogy between SEE and sputtering. Schou's model cannot be considered as a true microscopic model because it makes use of macroscopic quantities as input data (stopping power of electrons, energy

deposition law for electronic excitations). Its major advantage is that it can be used for a very wide range of incident particles and target materials.

Bennett and Roth¹⁴ have solved the Bethe-Rose-Smith (BRS) form¹⁷ of the Boltzmann equation by finite differences. They have shown that taking into account the primary-electron transport and backscattering, instead of using a simple straight-ahead path model, could increase the SE yield δ by a factor of 2. They assumed that the internal electrons are produced by the primaries through a screened Coulomb interaction and the transport mean free path (MFP) for the primaries was taken from Ref. 17.

Chung and Everhart¹⁵ have put in evidence the role of plasmon decay in the SEE from polycrystalline Al targets. Because the primary electrons were assumed to follow a straight-ahead path with no energy loss along the SE escape zone, the yield they calculated has to be compared to the partial yield δ_0 due to the ingoing primaries only, thus neglecting backscattering effects. The excitation function consists in bulk and surface plasmon contributions and in individual collisions with the conduction electrons. The decay of plasmons results from nearly vertical interband transitions and is described in a two-band model. As done by Berglund and Spicer¹⁸ for photoemission, they assumed that, during its transport to the surface, an excited electron could suffer only zero or one inelastic collision. No electron multiplication by cascade effects was taken into account.

The work done in Nantes by Cailler¹⁹ and Ganachaud²⁰ has mostly been devoted to the modelization of the electron interaction cross sections in metals. They have mainly used a Monte Carlo simulation code to describe the transport and escape of electrons.²¹ For polycrystalline Al targets,^{20,22,23} they calculated the elastic cross section by the partial-wave expansion method²⁴(PWEM) using a muffin-tin potential taken from Smrcka.²⁵ They described the conduction-electron gas by the Lindhard dielectric function²⁶ and the ionizing collisions by the classical formulation of Gryzinski.²⁷ They took approximately the surface collective excitations into account. Their main results are the electron yields δ and η for low-energy incident electrons ($E \approx 100$ eV–1 keV) on polycrystalline Al targets and the energy and angular distributions of the true secondary and backscattered electrons.²³ They have put in evidence the role of bulk and surface plasmon damping on the SEE characteristics.^{23,28,29} They found a satisfactory agreement with experimental results. They also extended their work to the SEE from noble metals,^{20,28,30} and in Refs. 31–34, they analyzed the Auger emission of Al, discussing the escape process and the shape of the L_{23} VV Auger line.

The interest of Shimizu and co-workers in SEE and Auger emission is more than 20 years old. They developed several Monte Carlo codes dedicated to the energy deposition of incident electrons, to the emission of secondary and Auger electrons, and to scanning electron microscopy.^{35–42} The paper by Koshikawa and Shimizu³⁵ can still be considered as a classical reference. In a recent work,³⁷ they calculated the elastic-scattering cross section by PWEM using the analytical expressions given

by Bonham and Strand for Thomas-Fermi-Dirac⁴³ and Hartree-Fock⁴⁴ potentials. They also developed an original use of Gryzinski's excitation function²⁷ for conduction electrons, based on the work of Krefting and Reimer⁴⁵ by defining a mean binding energy for the band. The approach used in this paper was applied to several elements in Refs. 38–41 and extended to compound materials in order to estimate the electron-backscattering effect in Auger electron spectroscopy. Recently, Ding and Shimizu⁴² used measurements of the optical loss function $\text{Im}[-1/\epsilon(0,\omega)]$ in order to modelize the interactions of incident electrons with the valence-conduction bands of Si, Cu, and Au targets. They applied their model to electron backscattering, Auger electron spectroscopy, and SEE. Their calculations are in good general agreement with experiments.

Bindi, Keller, Lantéri, and Rostaing in Nice have studied SEE and the electron transmission through thin films by solving numerically the Boltzmann equation by finite differences. In Ref. 46, they used elastic collision MFP's taken from Ref. 20 for Al and energy-range relationships deduced from the experimental results of Rostaing.⁴⁷ For the incident electrons, they solved a BRS form¹⁷ of the Boltzmann equation in order to calculate the backscattering characteristics of thick Al, Ag, and Cu targets⁴⁸ as well as the transmission and backscattering coefficients η_T and η_R for thin Al targets.⁴⁹ The more "classical" form of the Boltzmann equation was retained to study the SE transport. This model was extended in Ref. 50 to SEE from Cu and Au targets. As done by Cailler and Ganachaud,⁵¹ the source function is deduced from the optical loss function $\text{Im}[-1/\epsilon(0,\omega)]$ taken from Wehenkel.⁵² For the elastic collisions, the differential section is a screened Rutherford one with a screening parameter deduced from the MFP given in Ref. 20. More elaborate sets of cross sections were used in Refs. 53 and 54 for polycrystalline Al targets. The interactions with the jellium were modeled by an improved form of the Lindhard function,²⁶ i.e., Mermin's function⁵⁵ (see Sec. III B 1). Using this model, they studied the fine structure superimposed on the energy spectrum of the transmitted and backscattered electrons. We have to point out their interesting study of the influence of the reduced decay time γ in Mermin's model⁵⁵ on the transmitted and backscattered energy spectra.

Rösler and Brauer in Berlin have calculated the characteristics of electron- and proton-induced electron emission from polycrystalline Al targets. In Refs. 56 and 57, they have given a general theory for nearly-free-electron (NFE) metals and applied it to the SEE characteristics of polycrystalline Al targets. Their treatment of primary electrons uses simplifying assumptions. They approximate the primary trajectory (in the 1–2 keV range) by a straight-line path. SE's excited by the primaries are described by means of an excitation function $S(\mathbf{k}_0, \mathbf{k})$. They consider three mechanisms for electron excitations. The L -shell core electrons are excited via unscreened Coulomb interactions. These core states are represented by Bloch sums and the excited states are described by orthogonalized plane waves (OPW's).⁵⁸ The conduction electrons are excited due to screened

electron-electron collisions, the screening function being the Lindhard dielectric function.²⁶ Finally, electrons can be excited by decay of plasmons via interband transitions described in a model potential scheme.^{59,60} The above description was extended to incident protons^{61,62} and generalized in Refs. 63 and 64. The transport of SE's is described by the "infinite medium slowing down" model introduced by Wolff²⁰ for SEE. In this model, the internal electron source and the internal electron flux are uniform. The electrons slow down and multiply as if the medium were infinite. The elastic-scattering cross section is evaluated from the phase shifts calculated by Pendry⁶⁵ in a muffin-tin scheme. They also consider inelastic collisions with the jellium in the frame of the Lindhard dielectric function.²⁶ They obtained results in good agreement with experiments. For incident electrons, the yield they calculate is the partial yield δ_0 due to the penetrating primaries. They have clearly shown the importance of plasmon excitation and damping processes in SEE. From their calculations, it appears that the most important contribution to δ_0 in the 1–2 keV energy range is due to the core electron excitations. Larger contributions can be obtained when the OPW formalism⁵⁸ is substituted to the classical formula of Gryzinski.²⁷ They have also shown the crucial influence of the elastic collisions on the internal electron angular distribution flux, the effect being to render this distribution more isotropic. Good results have also been obtained for the electron yield γ in the case of incident protons. Recently,⁶⁶ they have emphasized the importance of dynamic screening on the calculated ratio of the electron yield to the stopping power for protons incident on polycrystalline Al. At last, they have shown that the inner-shell processes are dominant for electrons in the 1–10 keV range and for protons above a few MeV.⁶⁷

Devooght, Dubus, and Dehaes in Brussels have developed approximate solutions of the Boltzmann equation designed for SEE induced by electrons and protons.^{3,7,68} In the "improved age-diffusion model,"^{69,70} the internal electron source is first calculated separately. The Boltzmann equation for the SE's is then solved in the P_1 approximation after replacing the true scattering kernel by a "synthetic kernel."⁷¹ They used approximations similar to those of the Fermi age theory⁷¹ in order to obtain an analytical expression of the Green's function of the problem. For Al targets, their interaction model is quite similar to that given in Ref. 22 but neglecting ionizing collisions. They obtain rather good results for SEE from polycrystalline Al targets. Their second approach, the "transport-albedo" model,^{72,73} is an improved version of the "infinite medium slowing down" model,^{10,56,57} corrected in order to take into account the partial reflection boundary condition at the vacuum-medium interface by using the formalism of radiative transfer of Chandrasekhar.⁷⁴ They applied this model to the electron emission induced by low-energy protons incident on polycrystalline Al targets and obtained rather good results for the electron yield and energy spectrum. Recently,⁷⁵ they have introduced an integral transport correction model that corrects the "infinite medium slowing down" model by using a first-order collision expansion

for the correction flux. The results are in rather good agreement with Monte Carlo calculations.

From our description of the most recent theoretical models of SEE, it appears that a wide variety of assumptions have been used and for the charged-particle interactions in the target and for the transport description of the incident particles and of the SE's. A summary of the assumptions of the different groups is given in Table I. It is intricate to make a direct comparison between the various theoretical models due to the different sets of cross sections, the various necessary simplifying assumptions introduced to make calculations tractable in a given model, the way the transport process itself has been described, etc. The comparison to experiments has also to be made carefully. Let us remark that, while rather elaborate models have been given for the interaction cross sections, this has only been possible for NFE metals, and in practice, essentially for polycrystalline Al. A similar state of achievement has still to be reached for other materials.

III. INTERACTION CROSS SECTIONS FOR LOW-ENERGY ELECTRONS IN POLYCRYSTALLINE ALUMINUM TARGETS

In our calculations, polycrystalline Al is described in a radium-jellium model (this assumption is implicit in the works of all authors). The electrons interact inelastically with the jellium, i.e., the gas of delocalized conduction electrons. They also interact elastically and inelastically (by ionizing collisions) with the randomly distributed ionic cores, which constitute the radium.

These three types of collisions will be examined successively in the following sections for electrons in the 10 eV–1 keV range.

A. Elastic collisions

Internal electrons interact elastically with the ionic cores. The role of elastic collisions in SEE has been put in evidence by Ganachaud and Cailler,^{22,23} among others. For most authors, in the SE energy range ($E \approx 10$ –100 eV), the potential around each ion is central. A screened Rutherford cross section has sometimes been used, though it is only strictly valid for higher energies. In a recent review, Jablonski⁷⁶ emphasized the importance of the elastic collisions in Auger electron spectroscopy and x-ray photoelectron spectroscopy, but he only considered free-atom potentials. It has been shown^{77,78} that below 100 eV, i.e., typically in the SE energy range, the difference between free-atom potentials and solid-state potentials is drastic, indicating that free-atom potentials become rather questionable in the low-energy range. A convenient way to describe electron states and scattering in solids is to use "muffin-tin" potentials.⁷⁹ In the following, we shall just give a very brief description of the non-relativistic PWEM method and of the screened Rutherford formula. More detailed information can be found in Ref. 7.

1. Partial-wave expansion method and screened Rutherford formula

In the PWEM description, a particle of energy $E = \hbar^2 k^2 / 2m$ suffers a deflection by an angle θ with a

TABLE I. Summary of the interaction models, transport descriptions, and applications of some important groups specialized in electron emission problems. The description is of course not exhaustive. Most models have much evolved in course of time. The references are given in the text.

Group	Nantes M. Cailler and J. P. Ganachaud	Osaka R. Shimizu and co-workers	Nice R. Bindi, P. Keller, H. Lantéri, and P. Rostaing	Berlin M. Rösler and W. Brauer	Brussels A. Dubus, J. Devooght, and J. C. Dehaes
Applications	SEE Auger electrons	SEE, Auger electrons Electron penetration	SEE, backscattering, and transmission	SEE	SEE
Targets	Aluminum Metallic targets	Metallic targets Compound materials	Aluminum Metallic targets	Aluminum	Aluminum
Electron transport	Monte Carlo code	Monte Carlo code	Boltzmann equation "splitting-up" method	Boltzmann equation "infinite medium slowing down" model	Boltzmann equation "age-diffusion" model "transport-albedo" model
Electron interactions					
Elastic collisions	PWEM Smrcka's potential	Relativistic PWEM atomic potentials	PWEM Smrcka's potential	PWEM Pendry's potential	PWEM Smrcka's potential
Jellium	Lindhard	Lindhard, Gryzinski	Lindhard, Mermin	Lindhard	Lindhard
Inner shells	Gryzinski	Gryzinski	Gryzinski	OPW formalism	
Surface description	Surface plasmons thin zone				

differential scattering cross section $\sigma(\theta)$ given by

$$\sigma(\theta) = \frac{1}{k^2} \left| \sum_{l=0}^{\infty} (2l+1) e^{i\delta_l} \sin\delta_l P_l(\cos\theta) \right|^2, \quad (3.1)$$

where P_l is the l th order Legendre polynomial and δ_l the corresponding phase shift. The total scattering cross section is then given by

$$\sigma_{\text{el}} = 2\pi \int_0^\pi \sigma(\theta) \sin\theta d\theta = \frac{4\pi}{k^2} \sum_{l=0}^{\infty} (2l+1) \sin^2\delta_l, \quad (3.2)$$

and the elastic MFP is given by

$$\lambda_{\text{el}} = (N_{\text{ion}} \sigma_{\text{el}})^{-1}, \quad (3.3)$$

where N_{ion} is the density of ionic cores. A very often used form for the elastic-scattering cross section is the well-known screened Rutherford scattering formula introduced by Wentzel in 1927.⁸⁰ The differential cross section for one ionic core of charge Z is

$$\sigma_R(\theta) = \frac{Z^2 e^4}{(4\pi\epsilon_0)^2} \frac{1}{4E^2} \frac{1}{(1+2\beta - \cos\theta)^2}, \quad (3.4)$$

where β is the screening parameter. The total scattering cross section is given by

$$\sigma_R = 2\pi \int_0^\pi \sigma_R(\theta) \sin\theta d\theta = \frac{Z^2 e^4}{(4\pi\epsilon_0)^2} \frac{1}{4E^2} \frac{\pi}{\beta(1+\beta)}. \quad (3.5)$$

The whole problem for the Rutherford cross section is the choice of β . These aspects have been discussed thoroughly in Ref. 7. As previously done by Bindi, Lantéri and Rostaing,⁵⁰ in the present work, β has been deduced for polycrystalline Al from a given elastic MFP

$\lambda_{\text{el}}(E)$ by

$$\beta(1+\beta) = 1656.6 \frac{\lambda_{\text{el}}(\text{\AA})}{[E(\text{eV})]^2}, \quad (3.6)$$

where $\lambda_{\text{el}}(E)$ has been chosen as the elastic MFP calculated by the PWEM method from Smrcka's potential.²⁵

We compare in Fig. 1 the differential elastic-scattering cross sections (in polar diagram) for several incident-electron energies. Curves are normalized by $\int_0^\pi f(\theta) \sin\theta d\theta = 1$. The Smrcka scattering cross section shows structures which are absent from the monotonous Rutherford one. In the whole energy range, the former one is more forward peaked than the second one. This has, as is shown further, important consequences on the SEE yields either in backscattering or in transmission.

B. Inelastic interactions with the jellium

Much work has been done to calculate the inelastic interactions of charged particles in solids within the dielectric formalism. The wave number and frequency-dependent dielectric function $\epsilon(k, \omega)$ describes the response of the medium to an external point charge.⁸¹

The differential inverse mean free path (DIMFP) for an electron of energy E is given by⁸¹

$$\frac{d^2(1/\lambda)}{d\omega dk} = \frac{me^2}{4\pi^2\epsilon_0\hbar E} \frac{1}{k} \text{Im} \left[-\frac{1}{\epsilon(k, \omega)} \right], \quad (3.7)$$

where $\hbar\omega$ is the energy, $\hbar k$ is the momentum transfer, and $\text{Im}[-1/\epsilon(k, \omega)]$ is the energy-loss function.

The most popular dielectric function for the electron gas has been given by Lindhard.²⁶ It describes adequately the NFE materials such as Al. Many authors have tried to improve the Lindhard dielectric function by in-

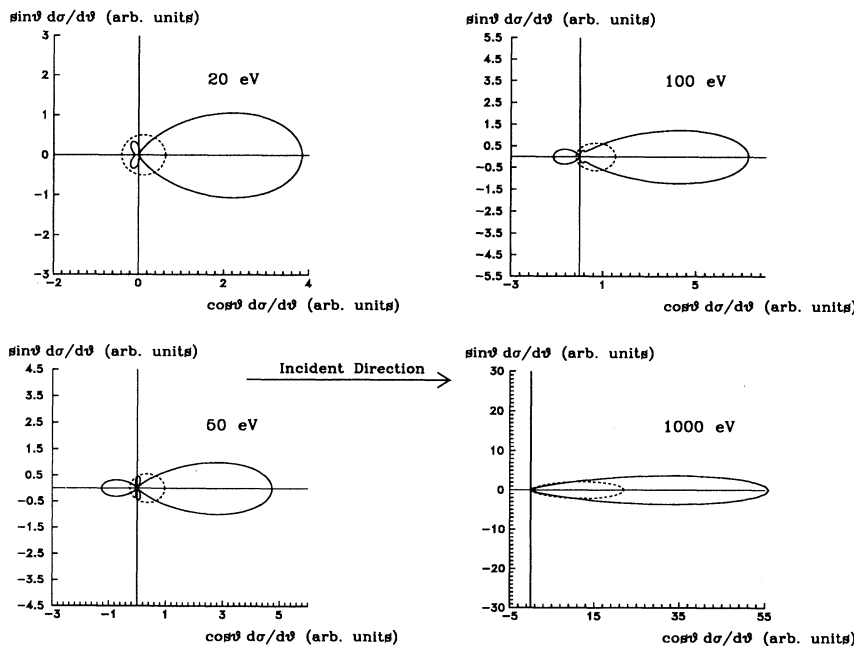


FIG. 1. Comparisons of angle differential elastic cross sections for various electron energies. Solid curves are for the Smrcka potential (Ref. 25) and dashed curves are for screened Rutherford cross sections with the same mean free path. Curves are normalized.

roducing a finite lifetime for the elementary excitations⁵⁵ or by taking exchange and correlation effects into account.^{82,83}

In the following, we describe the Lindhard function, the corrections for exchange and correlation, and the correction that takes into account a finite lifetime for the elementary excitations. Then, we indicate the way the different dielectric functions can be introduced in the calculations. We compare the characteristics of the corresponding inelastic MFP's and analyze their possible influence on SEE.

1. Random-phase approximations

Conduction electrons in polycrystalline Al behave approximately as free particles in a positive uniform background. The simplest expression for the dielectric response of a free-electron gas is the Hartree-Fock approximation (HFA).⁸¹ Coulomb interactions between target electrons are neglected. This gives rise to⁸¹

$$\frac{1}{\epsilon_{\text{HFA}}(k, \omega)} = 1 + U(k)\chi_0(k, \omega), \quad (3.8)$$

where $U(k) = e^2/\epsilon_0 k^2$ and $\chi_0(k, \omega)$ is the free-electron polarizability.

The true electrostatic potential in the medium $\varphi(\mathbf{k}, \omega)$ differs from $\varphi_{\text{ext}}(\mathbf{k}, \omega)$ by the induced potential $\varphi_{\text{ind}}(\mathbf{k}, \omega)$ given by

$$\begin{aligned} \varphi_{\text{ind}}(\mathbf{k}, \omega) &= \varphi(\mathbf{k}, \omega) - \varphi_{\text{ext}}(\mathbf{k}, \omega) \\ &= \frac{\varphi_{\text{ext}}(\mathbf{k}, \omega)}{\epsilon_{\text{HFA}}(k, \omega)} - \varphi_{\text{ext}}(\mathbf{k}, \omega) \\ &= U(k)\chi_0(k, \omega)\varphi_{\text{ext}}(\mathbf{k}, \omega). \end{aligned} \quad (3.9)$$

The HFA is a very rough approximation. A much better approximation replaces in Eq. (3.9) the external

potential $\varphi_{\text{ext}}(\mathbf{k}, \omega)$ by the true electrostatic potential $\varphi(\mathbf{k}, \omega)$. This is the random-phase approximation⁸¹ (RPA) and

$$\chi_{\text{RPA}}(k, \omega) = \frac{\chi_0(k, \omega)}{1 - U(k)\chi_0(k, \omega)} \quad (3.10)$$

and

$$\epsilon_{\text{RPA}}(k, \omega) = 1 - U(k)\chi_0(k, \omega). \quad (3.11)$$

As is obvious from the form of Eq. (3.10), the HFA approximation is a first-order approximation, while RPA takes higher-order polarization processes into account.

The effect of short-range interactions is to surround each electron by a depletion of negative charge. This can be accounted for by a factor $1 - G(k)$ that lowers the influence of the induced potential in Eq. (3.10). Hence Eq. (3.10) is modified, giving rise to an electron polarizability including the exchange and correlation effects

$$\chi_{\text{exc, cor}}(k, \omega) = \frac{\chi_0(k, \omega)}{1 - [1 - G(k)]U(k)\chi_0(k, \omega)}. \quad (3.12)$$

This subject has been thoroughly reviewed by Kugler⁸² and Mahan,⁸³ for instance. Vashishta and Singwi⁸⁴ gave for $G(k)$ the form

$$G(k) = A(1 - e^{-B(k/k_F)^2}) \quad (3.13)$$

and, for Al, $A = 0.895$ and $B = 0.336$. More involved forms of exchange and correlation corrections replace the static function $G(k)$ by a dynamic complex function $\tilde{G}(k, \omega)$.^{85,86}

Another important modification of the Lindhard function has been introduced by Mermin⁵⁵ in order to take into account the finite lifetime τ of the elementary excitations according to the following expression:

$$\epsilon_M(k, \omega) = \epsilon_{\tau, \text{RPA}}(k, \omega) = 1 + \frac{(1 + i/\omega\tau)[\epsilon_{\text{RPA}}(k, \omega + i/\tau) - 1]}{1 + i/\omega\tau[\epsilon_{\text{RPA}}(k, \omega + i/\tau) - 1]/[\epsilon_{\text{RPA}}(k, 0) - 1]}. \quad (3.14)$$

In the present paper, we limit ourselves to the comparison between the dielectric functions of Lindhard,²⁶ and Mermin,⁵⁵ and Vashishta and Singwi.⁸⁴ This will, however, allow us to check the influence of the important physical phenomena without focusing on untractable calculations.

2. Properties of the dielectric functions

As is well known, the elementary excitations in a free-electron gas can be split into collective and screened individual excitations. The two types of excitations are clearly distinguished in the framework of the Lindhard dielectric function.⁸¹ The bulk plasmons are well-defined excitations from $k=0$ up to the cutoff value k_c where the plasmon dispersion line $\omega = \omega_{\text{pl}}(k)$ [equivalent to $\epsilon(k, \omega) = 0$] enters the individual excitation zone. Beyond this limit, one can consider that a plasmon decays immediately by the creation of one electron-hole pair in the conduction band. When one uses a real function $G(k)$ to

include the exchange and correlation effects, the clear separation between individual and collective excitations still persists. The plasmon dispersion relation is, however, slightly modified.²⁰ When considering a finite lifetime for elementary excitations, the situation is more complex. In order to characterize the plasmon line, it is better to take, for each value of k , the value of ω which maximizes $\text{Im}[-1/\epsilon_M(k, \omega)]$. The plasmon line has now a finite linewidth $\Delta E_{1/2}(k)$ and one can use the following approximation:

$$\text{Im} \left[-\frac{1}{\epsilon_M(k, \omega)} \right] \approx \frac{A(k)[\Delta E_{1/2}(k)]^2}{4\hbar^2[\omega - \omega_M(k)]^2 + [\Delta E_{1/2}(k)]^2}. \quad (3.15)$$

Hence, $\omega = \omega_M(k)$ represents the plasmon dispersion relation. The damping of excitations can be characterized by the factor γ such that

$$\gamma = \frac{1}{\omega_{pl}(0)\tau} = \lim_{k \rightarrow 0} \frac{\Delta E_{1/2}(k)}{\hbar\omega_M(k)}, \quad (3.16)$$

where τ is the lifetime of the elementary excitations and $\omega_{pl}(0) = \sqrt{Ne^2/\epsilon_0 m}$ is the classical plasma frequency.

Ganachaud²⁰ tried to give an estimation for γ . He proposed $\gamma = 0.1$ as a good compromise to fit both the experimental width $\Delta E_{1/2}(0) = 0.5$ eV and the overall shape of the plasmon line for several values of k .^{87,88} We have used this value in our calculations.

It appears that the plasmon lines calculated from the Lindhard,²⁶ Mermin,⁵⁵ and Vashishta-Singwi⁸⁴ dielectric functions are quite similar.

More important differences appear between the electron interaction MFP's both for individual and collective excitations. The inverse mean free path (IMFP) for binary electron-electron collisions is given at energy E by

$$\frac{1}{\lambda_{ee}(E)} = \frac{1}{\pi a_0 E} \int_0^E \varphi(\omega) d(\hbar\omega), \quad (3.17)$$

where $\varphi(\omega)$ is the loss function defined by

$$\varphi(\omega) = \int_{k_-}^{k_+} \frac{1}{k} \text{Im} \left[-\frac{1}{\epsilon(k, \omega)} \right] dk, \quad (3.18)$$

where $k_+(\omega)$ and $k_-(\omega)$ are the values of the wave number k which limit the individual excitation zone. Their expressions have been given in Ref. 89. For the Lindhard²⁶ or the Vashishta-Singwi⁸⁴ dielectric functions, the plasmon excitation IMFP is calculated from^{20,89}

$$\frac{1}{\lambda_{pl}(E)} = \frac{1}{a_0 E} \oint_{\text{plasmon line}} \frac{1}{k} \frac{1}{|\partial \epsilon_1(k, \omega) / (\partial k)|} d\hbar\omega, \quad (3.19)$$

where $\epsilon_1(k, \omega)$ is the real part of the dielectric function $\epsilon(k, \omega)$. The integration is performed along the plasmon dispersion line $\omega = \omega_{pl}(k)$ between the limit $\hbar\omega_{\min}$ and $\hbar\omega_{\max}$.^{20,89}

For the Mermin function,⁵⁵ the plasmon line has a finite linewidth and the IMFP can be evaluated from

$$\frac{1}{\lambda_{pl}(E)} = \frac{1}{\pi a_0 E} \int_0^{k_c} \frac{dk}{k} F(k, E), \quad (3.20)$$

where

$$\begin{aligned} F(k, E) &= \int_{\hbar\omega_1(k)}^{\hbar\omega_2(k)} \frac{A(k) [\Delta E_{1/2}(k)]^2}{4\hbar[\omega - \omega_M(k)]^2 + [\Delta E_{1/2}(k)]^2} d\hbar\omega \\ &= \frac{A(k) \Delta E_{1/2}(k)}{2} \arctan \left[\frac{2\hbar[\omega - \omega_M(k)]}{\Delta E_{1/2}(k)} \right]_{\omega_1(k)}^{\omega_2(k)}, \end{aligned} \quad (3.21)$$

where $\omega_1(k)$ and $\omega_2(k)$ are suitable integration limits.²⁰

The MFP's for individual electron and plasmon excitations are compared in Figs. 2 and 3. For plasmon excitations, the MFP becomes larger when the Lindhard function is replaced by the Mermin one and still increases when the Vashishta-Singwi function is used. For electron-electron collisions, this order is reversed.

The total inelastic MFP in the jellium is obtained from

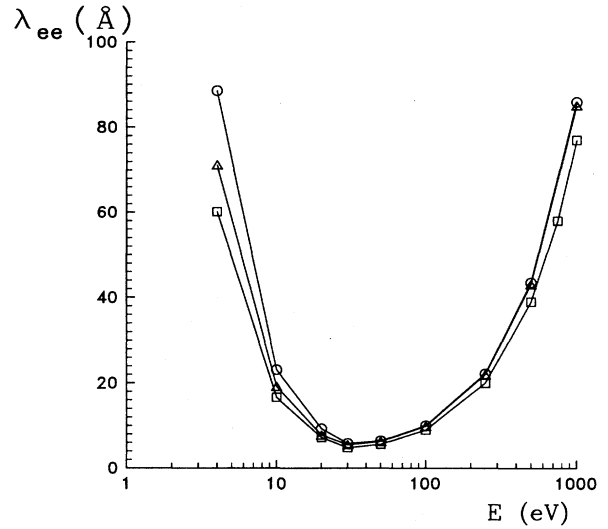


FIG. 2. Binary electron-electron collision mean free paths calculated from the Lindhard function (Ref. 26) (\circ), the Vashishta-Singwi function (Ref. 84) (\square), and the Mermin function (Ref. 55) (\triangle).

$$\lambda_{in}(E) = \frac{\lambda_{ee}(E)\lambda_{pl}(E)}{\lambda_{ee}(E) + \lambda_{pl}(E)}. \quad (3.22)$$

The inelastic MFP's for the three dielectric functions are compared in Fig. 4. One observes that, in the SE energy range ($E \leq 50$ eV), the inelastic MFP is larger for Lindhard's version than for that of Mermin and Vashishta and Singwi, while above 50 eV, this order is reversed. The important consequences of such differences on the computed values of yields will be thoroughly examined in Sec. IV B.

3. Excitation of secondary electrons and bulk plasmon damping

The calculated SEE yields are mostly sensitive to the values of the MFP's, i.e., integrated values, but are much

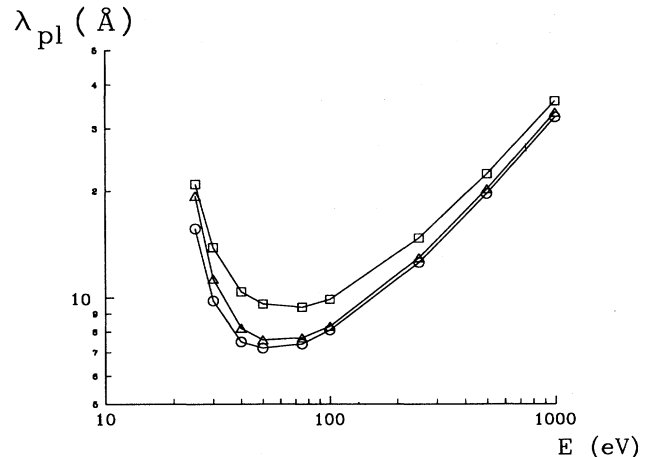


FIG. 3. Plasmon excitation mean free paths calculated from the Lindhard function (Ref. 26) (\circ), the Vashishta-Singwi function (Ref. 84) (\square), and the Mermin function (Ref. 55) (\triangle).

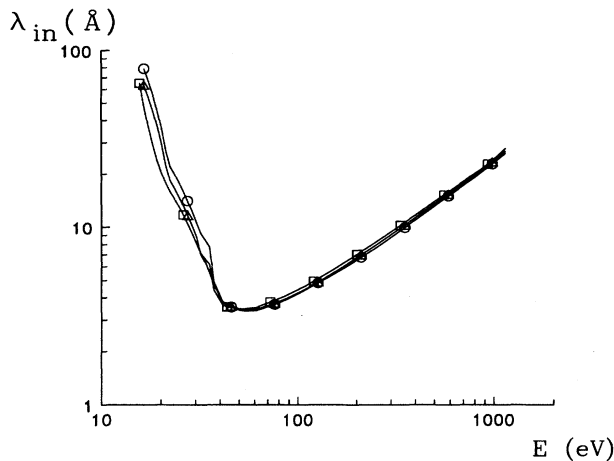


FIG. 4. Inelastic mean free paths in the free-electron gas calculated from the Lindhard function (Ref. 26) (○), the Vashishta-Singwi function (Ref. 84) (□), and the Mermin function (Ref. 55) (△).

less sensitive to the differential aspects of the interactions and excitations of electrons (energy and momentum transfers), which can be computed from $\text{Im}[-1/\epsilon(k, \omega)]$ and $\varphi(\omega)$. In the present calculations, these have only been evaluated from the Lindhard function.

Many papers have been devoted to the study of plasmon decay. The crystalline structure of the solid and the presence of a surface and impurities in the lattice are responsible for the damping of collective excitations.^{20,90} It has been shown by Hasegawa⁹⁰ that interband transitions are an important cause of plasmon decay. While plasmons can *a priori* decay via the excitation of more than one electron,²⁰ processes involving only *one* electron are preponderant.^{15,19,20} As already done Ganachaud and Cailler,^{20,22} we have assumed here that the probability of the excitation of one electron by plasmon damping is proportional to the density of the electron states in the valence-conduction band. Hence, the probability of the

excitation of one electron of energy E above the bottom of the conduction band is proportional to

$$\sqrt{E[E + \hbar\omega_{\text{pl}}(k)]}. \quad (3.23)$$

The dielectric functions considered here above are only valid for an infinite electron gas. Of course, for emission phenomena, the surface of the solid cannot be ignored. Roughly speaking,^{91,92} the plasmon dispersion relation $\epsilon(k, \omega)=0$ has to be replaced in the surface zone by $1 + \epsilon(k, \omega)=0$. This transformation affects a limited spatial zone at the vacuum-medium interface. For the sake of simplicity, it has been assumed in this paper that this zone extends from z_v in the vacuum to z_s in the solid.^{20,22} In this domain, the collective bulk excitations are simply replaced by purely surface excitations.

For practical calculations, it has been assumed that, in the surface zone, the plasmon creation MFP could be simply set equal to the bulk MFP [provided the energy is corrected by the difference between the classical bulk and surface plasmon energies: $\hbar\omega_{\text{pl}}(0) - \hbar\omega_{s,\text{pl}}(0)$]. The order of magnitude of z_s and z_v is 1 Å.²⁰ z_s and z_v can in fact be viewed as varying with the electron energy.⁹² Such aspects have not been considered in the present paper. Surface plasmons just as bulk plasmons have been assumed to decay by the creation of *one* excited electron from the conduction band.

C. Ionizing collisions

The interactions of charged particles with the electrons of the K and L inner shells of Al are generally considered apart from those with the conduction band.

Most authors have used the classical formulas of Gryzinski²⁷ In this treatment, an electron of energy E loses an energy amount ΔE by ionization according to the energy differential cross section

$$\sigma_i(E, \Delta E; U_i) = \frac{\sigma_0}{\Delta E^3} g_\sigma(x, y), \quad (3.24)$$

where $\sigma_0 = 656 \text{ eV}^2 \text{ \AA}^2$, $x = E/U_i$, $y = \Delta E/U_i$, U_i is the binding energy of the considered inner shell, and

$$g_\sigma(x, y) = \frac{1}{x} \left[\frac{1}{x+1} \right]^{3/2} \left[y \left[1 - \frac{1}{x} \right] + \frac{4}{3} \ln[2.718 + (x-y)^{1/2}] \right] \left[1 - \frac{y}{x} \right]^{1/(1+y)}. \quad (3.25)$$

The energy ΔE that an electron of energy E can lose varies between $U_i + E_F$ and $E - E_F$. Integrating Eq. (3.24) over ΔE practically gives the simple formula of Gryzinski,

$$\sigma_i(E; U_i) = \frac{\sigma_0}{U_i^2} \frac{1}{x} \left[\frac{x-1}{x+1} \right]^{3/2} \left[1 + \frac{2}{3} \left[1 - \frac{1}{2x} \right] \ln[2.718 + (x-y)^{1/2}] \right]. \quad (3.26)$$

For Al, the K shell, which has a binding energy of 1559 eV with respect to the Fermi level, plays no role at the primary energies considered in this paper. For the L shell, the L_1 subshell has two electrons with a binding energy of 118 eV and the L_{23} subshell has six electrons with a binding energy of 74 eV.

We compare in Tables II and III the electron inelastic MFP's and the stopping powers for interactions with the jellium and with the L shell. The ionizing collisions are much less frequent than the interactions with the jellium; nevertheless, their influence on the electronic stopping power is very important and even becomes preponderant

TABLE II. Comparison of inelastic mean free paths for electron interactions with the jellium (Mermin description) and with the L -shell electrons.

E (eV)	20	50	75	100	150	250	500	750	1000
$\lambda_{in}(E)$ (Å) (jellium)	7.1	3.4	3.9	4.5	5.7	8.2	13.8	19.0	24.0
$\lambda_{in}(E)$ (Å) (L shell)				276.0	126.0	93.0	103.0	127.0	151.0

above 500 eV. Their effect is to limit the penetration of the primaries in the target and to concentrate the electron source at moderate depths.

Rösler and Brauer⁶⁴ have used a quantum-mechanical description of the ionizing collisions. They showed that important differences with respect to Gryzinski's formulation²⁷ appear, especially on the energy distribution of the excited electrons. Such quantum-mechanical aspects were not considered in this work.

Holes created in inner shells can decay via Auger transitions (the fluorescence yield being here negligible). This Auger deexcitation has been presently accounted for.

IV. RESULTS

We study, in the following, the outgoing electron yields δ and η for electron emission in backscattering from thick Al targets and the backscattering and transmission coefficients η_R and η_T for incident electrons on thin Al targets. These yields have been evaluated only for normal incidence and obtained with a Monte Carlo simulation code. Several calculations have been made with various assumptions about the electron interaction cross sections. In all our calculations of δ and η , we have considered $N=10000$ primary-electron trajectories, whereas for η_R and η_T we have considered $N=25000$. The order of magnitude of the yields is unity; hence, a rough estimation of the relative statistical error is given by $1/\sqrt{N}$, which is presently 1%. This statistical aspect must be kept in mind when comparing yield values from different Monte Carlo calculations. We emphasize in the following the influence of the description of elastic scattering, the influence of the choice of the dielectric function, and the importance of ionizing collisions.

A. Influence of the description of elastic collisions

Our analysis of the influence of the elastic effect on the yields will deal with the three following aspects. First, we give some theoretical considerations based upon the Boltzmann equation. Second, we study the influence of the angular behavior of the elastic-scattering cross sec-

tion. For that, we shall compare the results obtained from Smrcka's potential²⁵ by a PWEM method, to those evaluated with a screened Rutherford formula (but adjusted so that it gives an identical value for the MFP). Third, we shall use a more overall approach, and check the influence of the multiplication, by a constant factor k , of the elastic MFP as a whole in the energy range considered.

1. Boltzmann equation

The role of elastic scattering in SEE is double. It influences strongly the penetration of the primary electrons in the target. It also plays a role in the transport of the SE's themselves, i.e., the electrons excited by the primaries or by the cascade process.

As described in Ref. 3, the transport of the primary and secondary electrons can be studied by solving the Boltzmann equation. In plane geometry, where the depth x is the only space variable, we obtain in the stationary case the total flux $\Phi_T(x, E, \mu)$ of the electrons with an energy E and moving in a direction $\mu = \cos\theta$ with respect to the x axis.

Two differential scattering cross sections appear in this equation. First, the true scattering cross section $\Sigma_s(E' \rightarrow E, \mu' \rightarrow \mu)$ gives the probability that an electron is scattered from (E', μ') to (E, μ) . It can be written as the sum of an inelastic and an elastic part:

$$\Sigma_s(E' \rightarrow E, \mu' \rightarrow \mu) = \Sigma_{el}(E', \mu' \rightarrow \mu) \delta(E - E') + \Sigma_{inel}(E' \rightarrow E, \mu' \rightarrow \mu). \quad (4.1)$$

Second, to take into account the excitation of electrons by collisions with the jellium and by ionizing collisions, the Boltzmann equation also includes an excitation cross sections $\Sigma_s^i(E' \rightarrow E, \mu' \rightarrow \mu)$. It gives the probability that an electron (E', μ') excites another electron at energy E in the direction μ . In terms of these cross sections, the Boltzmann equation can be written as

TABLE III. Electronic stopping power $S_e(E)$ for electron interactions with the jellium and with the L -shell electrons.

E (eV)	20	50	75	100	150	250	500	750	1000
$S_e(E)$ (eV/Å) (jellium)	1.91	6.14	5.66	5.06	4.12	2.91	1.64	1.17	0.91
$S_e(E)$ (eV/Å) (L shell)				0.31	0.78	1.28	1.44	1.30	1.16

$$\left[\mu \frac{\partial}{\partial x} + \Sigma_s(E) \right] \Phi_T(x, E, \mu) = \int_E^\infty \int_{-1}^{+1} [\Sigma_s(E' \rightarrow E, \mu' \rightarrow \mu) + \Sigma_s^s(E' \rightarrow E, \mu' \rightarrow \mu)] \Phi_T(x, E', \mu') dE' d\mu', \quad (4.2)$$

where $\Sigma_s(E') = \int_0^{E'} \int_{-1}^{+1} \Sigma_s(E' \rightarrow E, \mu' \rightarrow \mu) dE d\mu$ is the total scattering cross section (inverse mean free path) at energy E' .

For normal incidence of electrons (at energy E_p) the boundary condition is

$$\begin{aligned} \Phi_T(0, E, \mu) &= \delta(\mu - 1) \delta(E - E_p) \\ &+ H[\mu_c(E) - \mu] \Phi_T(0, E, -\mu) \quad (\mu > 0). \end{aligned} \quad (4.3)$$

The first term expresses the ingoing primary-electron flux, while the second term (the Heaviside step function) expresses the partial reflection of the internal electrons at

the surface. The critical cosine for escape $\mu_c(E) = \sqrt{U_0/E}$, where U_0 is the potential barrier at the surface.

The Boltzmann equation (4.2) with boundary condition (4.3) can in principle be solved directly to give the total electron flux. However, it is convenient to split the total flux $\Phi_T(x, E, \mu)$ in a primary-electron flux $\Phi_p(x, E, \mu)$ and a true secondary-electron flux $\Phi(x, E, \mu)$:

$$\Phi_T(x, E, \mu) = \Phi_p(x, E, \mu) + \Phi(x, E, \mu). \quad (4.4)$$

As is easily seen,³ Φ_p is the solution of Eq. (4.2) without the Σ_s^s creation cross section and satisfying the boundary condition (4.3). Once Φ_p is known, we can calculate Φ by solving Eq. (4.2), which includes now a source term $Q(x, E, \mu)$:

$$\left[\mu \frac{\partial}{\partial x} + \Sigma_s(E) \right] \Phi(x, E, \mu) = \int_E^\infty \int_{-1}^{+1} [\Sigma_s(E' \rightarrow E, \mu' \rightarrow \mu) + \Sigma_s^s(E' \rightarrow E, \mu' \rightarrow \mu)] \Phi(x, E', \mu') dE' d\mu' + Q(x, E, \mu), \quad (4.5)$$

with the partial reflection boundary condition

$$\Phi(0, E, \mu) = H[\mu_c(E) - \mu] \Phi(0, E, -\mu) \quad (\mu > 0) \quad (4.6)$$

and

$$\begin{aligned} Q(x, E, \mu) &= \int_E^\infty \int_{-1}^{+1} \Sigma_s^s(E' \rightarrow E, \mu' \rightarrow \mu) \\ &\times \Phi_p(x, E', \mu') dE' d\mu'. \end{aligned} \quad (4.7)$$

In most cases, the primary- and secondary-electron energy ranges are very different.³ Hence, the differential scattering cross sections are also very different (see, for instance, Fig. 1 for the elastic differential cross section). Hence, solving Eq. (4.2) directly for $\Phi_T(x, E, \mu)$ can be a very difficult task.

Considering separately the primary and secondary electrons greatly simplifies the problem because distinct techniques can be applied to calculate the both fluxes. In

the following, we will use this splitting in the discussion of the influence of the elastic collisions on both the primary- and secondary-electron fluxes.

In order to explain the influence of elastic scattering on the secondary-electron flux, we will use the "infinite medium slowing down" model.³ This model considers that both $Q(x, E, \mu) = Q_\infty(E, \mu)$ and $\Phi(x, E, \mu) = \Phi_\infty(E, \mu)$ are uniform, at least in the depth zone from which the secondary electrons can escape. This model has been used by several authors^{10,6} and gives rather good results³ though it has been shown in Ref. 75 that it overestimates the yield by about 30% for protons incident on polycrystalline aluminum targets. It is worth noting here that this model can only be used to solve the Boltzmann equation for secondary electrons and not for primary electrons.

With the assumption of uniformity of Q , and Φ , Eq. (4.5) becomes

$$\Sigma_s(E) \Phi_\infty(E, \mu) = \int_E^\infty \int_{-1}^{+1} [\Sigma_s(E' \rightarrow E, \mu' \rightarrow \mu) + \Sigma_s^s(E' \rightarrow E, \mu' \rightarrow \mu)] \Phi_\infty(E', \mu') dE' d\mu' + Q_\infty(E, \mu). \quad (4.8)$$

To solve this equation, we use the Legendre polynomial expansions

$$Q_\infty(E, \mu) = \sum_{l=0}^{\infty} \frac{2l+1}{2} Q_l(E) P_l(\mu), \quad (4.9)$$

$$\Phi_\infty(E, \mu) = \sum_{l=0}^{\infty} \frac{2l+1}{2} \Phi_l(E) P_l(\mu), \quad (4.10)$$

and

$$\Sigma_s(E' \rightarrow E, \mu' \rightarrow \mu) = \sum_{l=0}^{\infty} \frac{2l+1}{2} B_l(E' \rightarrow E) P_l(\mu) P_l(\mu'), \quad (4.11)$$

$$\Sigma_s^s(E' \rightarrow E, \mu' \rightarrow \mu) = \sum_{l=0}^{\infty} \frac{2l+1}{2} B_l^s(E' \rightarrow E) P_l(\mu) P_l(\mu'), \quad (4.12)$$

which give a slowing down equation for each angular order l :

$$\begin{aligned} \Sigma_s(E) \Phi_l(E) &= \int_E^\infty [B_l(E' \rightarrow E) + B_l^s(E' \rightarrow E)] \Phi_l(E') + Q_l(E). \end{aligned} \quad (4.13)$$

Since the scattering events are either elastic or inelastic, we can write

$$\Sigma_s(E) = \Sigma_{el}(E) + \Sigma_{inel}(E), \quad (4.14)$$

where $\Sigma_{el}(E) = 1/\lambda_{el}(E)$ is the elastic cross section (inverse mean free path) and $\Sigma_{inel}(E) = 1/\lambda_{inel}(E)$ is the inelastic cross section. From Eq. (4.1), we have

$$B_l(E' \rightarrow E) = \Sigma_{el}(E') \delta(E - E') \langle P_{l,el}(E') \rangle + B_{l,inel}(E' \rightarrow E), \quad (4.15)$$

where $B_{l,inel}(E' \rightarrow E)$ is the inelastic part of the true scattering kernel $B_l(E' \rightarrow E)$. $\langle P_{l,el}(E') \rangle$ is the average elastic moment at angular order l and its expression is

$$\Sigma_{el}(E') \langle P_{l,el}(E') \rangle = \int_{-1}^{+1} \Sigma_{el}(E', 1 \rightarrow \mu) P_l(\mu) d\mu. \quad (4.16)$$

We have obviously $\langle P_{0,el}(E') \rangle = 1$ and $|\langle P_{l,el}(E') \rangle| \leq 1$ for $l \geq 1$.

Introducing the above expressions in Eq. (4.13), we obtain

$$\begin{aligned} & \{ \Sigma_{inel}(E) + [1 - \langle P_{l,el}(E) \rangle] \Sigma_{el}(E) \} \Phi_l(E) \\ &= \int_E^\infty [B_{l,inel}(E' \rightarrow E) \\ & \quad + B_l^s(E' \rightarrow E)] \Phi_l(E') dE' + Q_l(E). \end{aligned} \quad (4.17)$$

As $\langle P_{0,el}(E) \rangle = 1$, one can see, by inspection of Eq. (4.17), that the elastic collisions have no influence on $\Phi_0(E)$ but that they influence the higher-order angular terms $\Phi_l(E)$. As explained in Ref. 68, it can be shown from Eq. (4.17) that increasing the elastic cross section or making it more isotropic decreases the value of $\Phi_l(E)$ (for $l \geq 1$). As a consequence, the influence of the elastic collisions on the angular flux $\Phi(E, \mu)$ is to make it more isotropic because $\Phi_0(E)$ remains unchanged. Hence, the influence of the elastic collisions on the true secondary yield δ , at least the part due to the transport of the internal excited SE, is only a second-order effect, since the internal SE source term $Q(E, \mu)$ is itself almost isotropic.⁹³

However, the effect of elastic collisions on the primary-electron transport and penetration is very important. In a first approximation, it can be considered that, in the primary-electron energy range, the inelastic collisions give rise to energy losses but to negligible angular deflections, while the elastic scattering events lead to angular deflections without energy losses. The penetration of the primaries in the target is limited both by their energy losses and by their angular dispersion due to multiple elastic scatterings. The so-called "transport MFP," well known in neutron transport theory,⁹⁴ can be introduced to characterize the loss of directivity suffered by the primary beam.

It can be easily deduced from the elastic MFP by introducing the following "synthetic" kernel (see Williams,⁷¹ for instance, to find information about the use of "synthetic" kernels, i.e., approximate cross sections with adjustable parameters that are used instead of the real cross

sections):

$$\Sigma_{el}^*(E' \rightarrow E, \mu' \rightarrow \mu) = \left[\frac{\Sigma_{tr}(E)}{2} + \Sigma_{fwd}(E) \delta(\mu - \mu') \right] \times \delta(E - E'). \quad (4.18)$$

This "synthetic" scattering kernel is made of two terms. The first one is the "transport" cross section [$\lambda_{tr}(E) = 1/\Sigma_{tr}(E)$ is the elastic "transport MFP"] that gives rise to the isotropic elastic scattering part, and the second one is the "forward" cross section that gives rise to no energy loss and no angular deflection. The anisotropy of the elastic cross section is then concentrated in $\Sigma_{fwd}(E)$, whereas the loss of directivity of the electrons is concentrated in $\Sigma_{tr}(E)$.

The elastic scattering kernel $\Sigma_{el}(E' \rightarrow E, \mu' \rightarrow \mu)$ can be approximated by the "synthetic" kernel $\Sigma_{el}^*(E' \rightarrow E, \mu' \rightarrow \mu)$.

In order that the "synthetic" kernel resembles most closely the original one, we adjust $\Sigma_{tr}(E)$ and $\Sigma_{fwd}(E)$ so that the first two angular moments $\langle P_{0,el}(E) \rangle$ and $\langle P_{1,el}(E) \rangle$ are the same for Σ_{el} and Σ_{el}^* . Hence, we obtain

$$\Sigma_{el}(E) = \Sigma_{tr}(E) + \Sigma_{fwd}(E), \quad (4.19)$$

$$\Sigma_{el} \langle P_{1,el}(E) \rangle = \Sigma_{fwd}(E). \quad (4.20)$$

The angular characteristics of the elastic collisions are now contained in a global way in both the "transport" and "forward" cross sections. Hence,

$$\lambda_{tr}(E) = \frac{1}{\Sigma_{tr}(E)} = \frac{\lambda_{el}(E)}{1 - \langle P_{1,el}(E) \rangle}. \quad (4.21)$$

The ratio $\Sigma_{el}(E)/\Sigma_{tr}(E) = \lambda_{tr}(E)/\lambda_{el}(E)$ gives an idea of the number of elastic collisions necessary for an impinging electron to lose the memory of its initial direction. We compare in Fig. 5 the transport MFP's deduced from the Smrcka potential and from the screened Rutherford

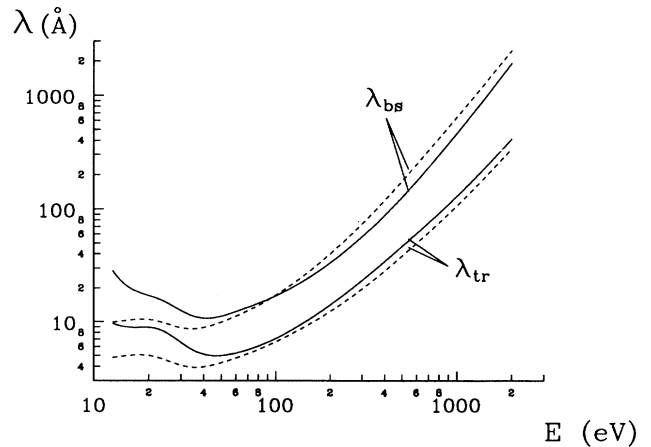


FIG. 5. Elastic transport mean free path λ_{tr} and elastic back-scattering mean free path λ_{BS} calculated from (solid line) the elastic mean free path deduced from the Smrcka potential (Ref. 25) and (dashed line) screened Rutherford cross section with the same mean free path as deduced from the Smrcka potential.

cross section (giving the same elastic MFP). The Smrcka transport MFP is larger, in the whole energy range, than the Rutherford one by a factor of about 1.3. Hence, using Smrcka's version for elastic scattering leads to a much deeper primary-electron penetration. The order of magnitude of $\lambda_{tr}(E)$, at $E = 1000$ eV, is of about 100 \AA . It gives a good estimate of the mean penetration depth of the primaries in the target. Let us notice that the transport MFP is about 10 times the elastic MFP at 1000 eV and that this number increases with electron energy. Some authors have used a so-called elastic backscattering cross section (see Ref. 32 for instance). To define it, only collisions giving rise to a reversal of the electron direction are considered. The corresponding MFP is almost one order of magnitude larger than the transport MFP in the primary-electron energy range considered (see Fig. 5). This elastic-backscattering MFP is not in fact the correct variable to be taken into account to describe the primary-electron penetration (and transmission) because it is a MFP for complete reversal of the electron direction and not a MFP for the loss of directivity of the electron.

2. Influence of the angular description of elastic collisions

We compare in Fig. 6 the yields δ and η obtained with both descriptions of the elastic scattering. The values of the backscattering coefficient η are slightly modified by the choice of elastic cross sections. Above 300 eV, η_{Ruth} is slightly larger than η_{Smrcka} .

The influence of the elastic collisions is much more evident on the true SE yield δ : δ_{Ruth} is larger than δ_{Smrcka} in the 100 – 500 eV range. As indicated above, the elastic collisions mostly influence the penetration of the incident primaries into the target. At 500 eV, the transport MFP $\lambda_{tr}(E) = 48 \text{ \AA}$ for the Smrcka description and $\lambda_{tr}(E) = 40 \text{ \AA}$ for the Rutherford one. These values are of the order

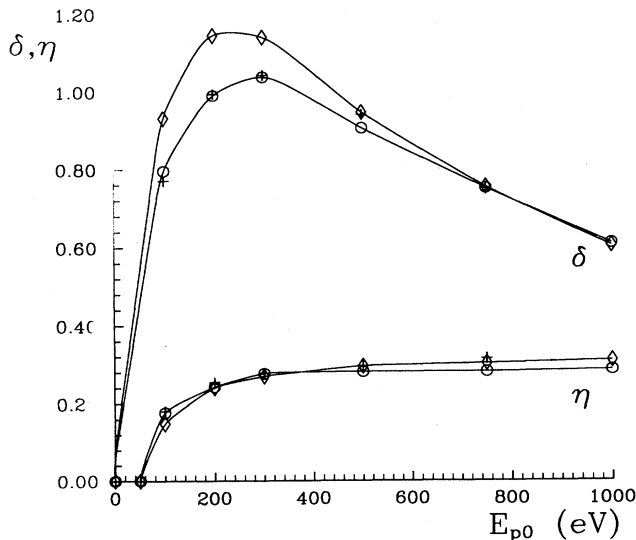


FIG. 6. Influence of the choice of the elastic cross section. δ and η yields as a function of the primary electron energy E_{p0} . Rutherford's description (\diamond) and Smrcka's description (Ref. 25) (\circ , $+$).

of magnitude of the depth from which the electrons can escape ($d \approx 50$ – 75 \AA for Al). As the transport MFP characterizes the limitation of the penetration of the incident primaries into the target due to elastic effects, below 500 eV, the SE source is mainly concentrated within this depth. In the Rutherford description, the electron source is concentrated closer to the surface and, as a consequence, the yield δ is enhanced. Above 500 eV, the transport MFP becomes larger than the depth from which the electrons can escape. Consequently, no significant difference between the δ yield values can appear.

The influence of the calculation of elastic collisions on the electron penetration is confirmed by the calculation of η_R and η_T yields for 1 -keV electrons incident on thin films (see Fig. 7). As shown for η , the η_R values are slightly larger for the Rutherford description than for the Smrcka description. The influence on η_R and η_T is more apparent as soon as the target thickness exceeds 75 \AA , i.e., the order of magnitude of the transport MFP for 1 -keV electrons.

In order to check more fully the influence of the angular description of the elastic collisions, we have made additional calculations by using some rather extreme assumptions on the angular behavior of the elastic collisions (while keeping the same elastic MFP): An isotropic and a completely forward-peaked cross section were used. In the former case, the transport MFP is equal to the elastic MFP. In the latter case, the elastic transport MFP is infinite.

The δ and η yields obtained using both assumptions are compared in Table IV to those obtained with the Smrcka and the Rutherford descriptions.

These results clearly indicate the strong influence of the angular behavior. For isotropic elastic collisions, the penetration of incident primaries into the target is very

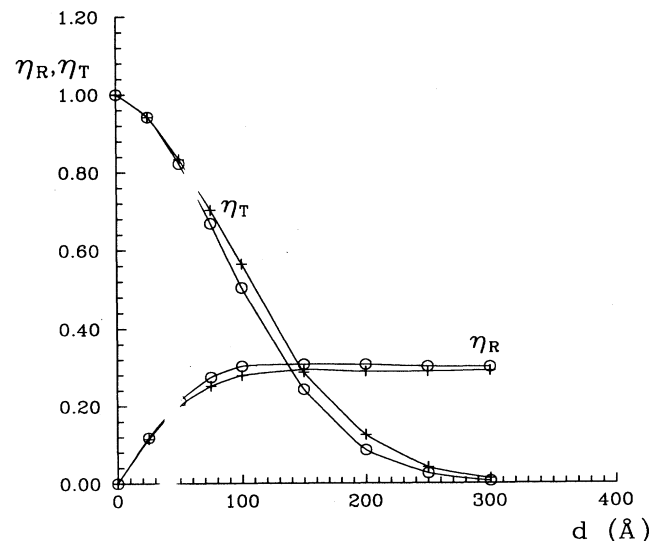


FIG. 7. Influence of the choice of the elastic cross section. η_R and η_T backscattering coefficients as a function of target thickness d for 1000 -eV incident electrons. Rutherford's description (\circ) and Smrcka's description (Ref. 25) ($+$).

TABLE IV. δ and η yields obtained using various angular descriptions of the elastic collisions. The ionizing collisions have been left out for these calculations ($z_v = z_s = 0.0 \text{ \AA}$).

E (eV)		50	100	200	300	400	500	600	800	1000
Smrcka description	δ	0.68	0.84	0.97	0.90	0.78	0.66	0.60	0.47	0.37
	η	0.00	0.17	0.26	0.29	0.29	0.30	0.31	0.31	0.32
Rutherford description	δ	0.77	1.01	1.06	0.98	0.81	0.70	0.61	0.45	0.37
	η	0.00	0.14	0.24	0.29	0.31	0.32	0.33	0.35	0.36
Isotropic collisions	δ	0.81	1.01	1.10	1.03	0.96	0.84	0.77	0.63	0.55
	η	0.00	0.22	0.42	0.52	0.59	0.62	0.66	0.71	0.74
Forward-peaked collisions	δ	0.12	0.41	0.52	0.47	0.42	0.35	0.30	0.23	0.18
	η	0.00	0.002	0.002	0.004	0.005	0.006	0.006	0.006	0.006

limited. Most incident primaries are backscattered and the δ yield is enhanced because these backscattered primaries give rise to an important electron source contribution very close to the surface. When elastic collisions are completely forward peaked (and thus play no role), the backscattering yield η is very low because only inelastic collisions are responsible for angular deflections of the incident primaries.

The δ yield is decreased because the backscattered primaries do not contribute any more to the excitation of electrons. When comparing the Rutherford and Smrcka descriptions, it is clear that the Rutherford description is closer to the isotropic case than the Smrcka description.

Apart from the comparisons dealing only with the angular aspects of the elastic collisions, we have made some tests about the influence of the magnitude of the elastic MFP by multiplying rather arbitrarily the elastic MFP by a constant factor k , ranging from 0.5 to 2.0.

The δ and η yields calculated with several values of k are compared in Table V. The influence of k is obvious: δ and η decrease as k increases. Multiplying the elastic MFP by a constant factor results in multiplying the transport MFP by the same factor. For k less than 1, the primary-electron penetration in the material is reduced. Hence, more primaries are backscattered and the true secondary yield δ is enhanced too.

As a conclusion, it appears that the description of elastic collisions influences strongly the calculated yields δ

and η through its influence on the primary-electron penetration. Moreover, the elastic scattering is globally well accounted for by using the Smrcka description. This is confirmed by the comparison of the calculated values of δ and η to experimental results (see Sec. IV D).

From the dependence of η_T on the target thickness d , one can roughly estimate the primary range R at $E_p = 1$ keV. Conventionally, this range is taken as the value of d for which $\eta_T = 0.01$.

Following Fitting,⁹⁵ R can be estimated from

$$R(E_p) = 900\rho^{-0.8}E_p^{1.3}, \quad (4.22)$$

where ρ is the density of the target, R is in \AA , and E_p in keV. Fitting's formula gives $R = 407 \text{ \AA}$ at $E_p = 1$ keV for Al targets. From the η_T values, we can roughly estimate that R ranges between 300 and 350 \AA using the Smrcka description. This is in rather good agreement with the value predicted by Fitting's formula.

B. Influence of the choice of the dielectric function

Changes in the dispersion relation or in the shape of the loss function $\varphi(\omega)$ influence mainly the electron spectrum in the characteristic energy-loss region. Integrated quantities such as the secondary yield δ or the backscattering coefficient η are much less sensitive to these rather differential features. This is the reason why the

TABLE V. δ and η yields calculated after multiplication of the elastic mean free path by a constant factor k . The ionizing collisions have been left out for those calculations ($z_v = z_s = 0.0 \text{ \AA}$).

E (eV)	100		300		600		1000	
k	δ	η	δ	η	δ	η	δ	η
0.50	0.99	0.26	1.25	0.38	1.01	0.39	0.71	0.39
0.75	0.90	0.22	1.16	0.31	0.96	0.32	0.69	0.33
1.00	0.87	0.17	1.10	0.27	0.90	0.28	0.66	0.29
1.50	0.79	0.13	1.00	0.22	0.87	0.23	0.62	0.24
2.00	0.70	0.11	0.98	0.20	0.81	0.20	0.59	0.21

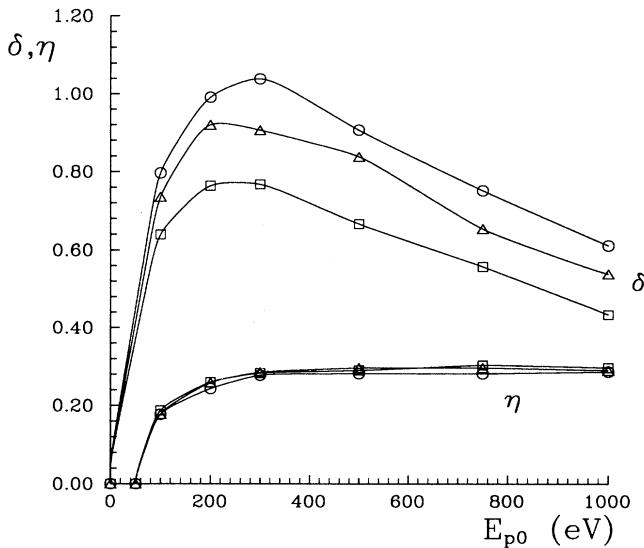


FIG. 8. Influence of the choice of the dielectric function. δ and η yields as a function of the primary-electron energy E_{p0} calculated from the Lindhard function (Ref. 26) (\circ), the Vashista-Singwi one (Ref. 84) (\square), and the Mermin one (Ref. 55) (\triangle).

only aspect we have studied here is the modification of the MFP values due to a particular choice of the dielectric function. Variations between dispersion relations or loss function shapes have been simply ignored.

We compare in Fig. 8 the electron yields δ and η obtained using the MFP's calculated from the three dielectric functions. The backscattering coefficient η is rather

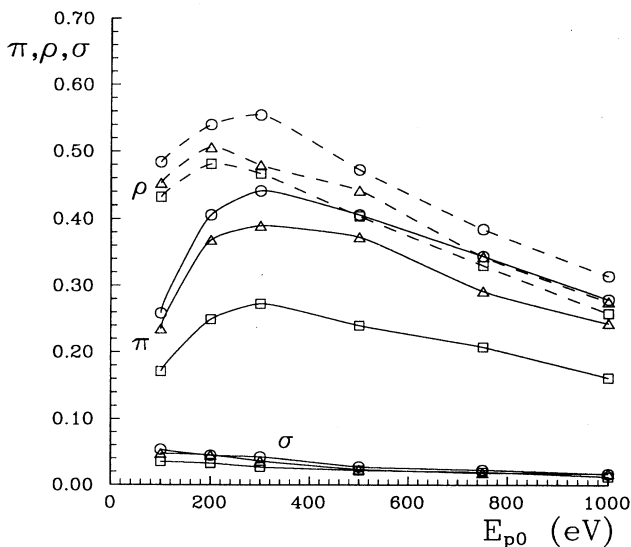


FIG. 9. Influence of the choice of the dielectric function. π , ρ , and σ partial yields as a function of E_{p0} calculated from the Lindhard function (Ref. 26) (\circ), the Vashista-Singwi one (Ref. 84) (\square), and the Mermin one (Ref. 55) (\triangle). π is the yield resulting from bulk plasmon decays, σ is the yield resulting from surface plasmon decays, and ρ is the rest of the δ yield.

insensitive to this choice. Indeed, above 50 eV, that is, in the region where the primary-electron transport is concerned, the inelastic MFP is not very sensitive to the dielectric function.

On the contrary, this choice strongly influences the true secondary yield δ , which is reduced by using the Mermin function instead of the Lindhard one and still further by using the Vashista-Singwi function. In fact, the reduction is almost independent of the incident-electron energy, the factor being approximately 0.9 when replacing the Lindhard function by the Mermin one and 0.85 when the Vashista-Singwi function is substituted for the Mermin one.

For a better understanding of the results presented in Fig. 8, we have separated the different contributions to the yield δ (see Fig. 9). The first one π comes from the electrons created by the volume plasmon decay. The second one σ is due to the electrons created by the surface plasmon decay. The rest has been labeled ρ . This latter contribution is mainly due to the electrons excited by individual collisions within the jellium but also to the electrons produced by the ionization of the inner shells and the subsequent Auger relaxation. In our calculations, the separation of δ into several contributions has been made by reference to the type of event which has directly led to the creation of an escaping electron. For Rösler and Brauer, the same label is assigned to an electron created by the primary beam and to the whole cascade it generates.

According to our calculations, the surface plasmon component σ is always small. The two others π and ρ are important and of similar magnitudes.

The influence of the choice of the dielectric function is much more important on π than on ρ .

The above results are clearly due to a MFP effect. The total inelastic MFP in the range $E \leq 50$ eV increases from the Vashista-Singwi function to the Mermin and then to the Lindhard one. For the SE's which have their energy within this domain, this results in an enhanced escape probability. One can, in a crude model, consider that the escape probability $P(x, E)$ for an electron of energy E , which has a distance x to travel before reaching the surface, is given by

$$P(x, E) \simeq e^{-x/\lambda(E)}, \quad (4.23)$$

where $\lambda(E)$ has been, in a rough approximation, taken as the inelastic MFP $\lambda_{in}(E)$ at the same energy. For $x = 10$ Å and $E = 10$ eV above the Fermi level (both values are representative of the escape depth and of the energy of the internal SE's), $\exp[-x/\lambda_{in}(E)] = 0.648$ for the Lindhard function, 0.594 for the Mermin one, and 0.547 for the Vashista-Singwi one. Their relative values are in good agreement with those calculated for δ .

When looking at the partial contributions π and ρ , the influence of the choice of the dielectric function on π is enhanced because, when going from the Vashista-Singwi function to the Mermin and then to the Lindhard function, the plasmon excitation cross section increases. Hence, less plasmons are created when using the Vashista-Singwi function instead of the two others and

π is much lower. On the contrary, for ρ , the increase of the electron-electron collision MFP gives rise to a compensation of the escape probability effect.

The η_R and η_T values are nearly independent of the choice of the dielectric function. This confirms that this latter influences essentially the escape of SE's.

C. Influence of ionizing collisions

We compare in Fig. 10 the δ and η yields calculated with and without including the ionizing collisions. The backscattering coefficient η is slightly decreased (by about 10% in the whole energy range considered) when including these collisions. The true secondary yield δ is much more influenced by them, for primary energies above 150 eV (this value corresponds to the inner-shell ionization threshold).

At 1 keV, δ is decreased by a factor of 2 when ionizing collisions are neglected. As indicated above, these collisions are rather infrequent events, but their contribution to the electronic stopping power is very important. This contribution even becomes preponderant at 1 keV.

For SEE, the influence of ionizing collisions is double, first on the penetration of primary electrons into the target and also as a source contribution.

This last role has been emphasized by Rösler and Brauer.⁶⁴ Their treatment of the ionizing collisions differs from ours as it is a quantum-mechanical treatment, while Gryzinski's formulation²⁷ is a classical one. In fact, what they have shown is that the ionizing collisions give the most important contribution to the partial electron yield δ_0 as the backscattering effects are treated apart in their work.

In order to compare our results with theirs, we have calculated δ_0 , and we obtained results close to theirs since, for instance, we could estimate that, at 1 keV, about 50% of the partial yield δ_0 is due to the ionizing

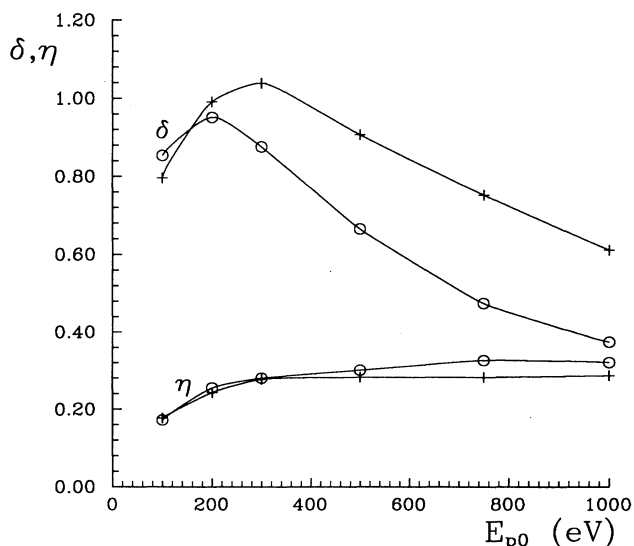


FIG. 10. Influence of the ionizing collisions. δ and η yields as a function of the primary electron energy E_{p0} calculated with (+) and without (o) ionizing collisions.

collision source.

We show in Fig. 11 the transmission and backscattering coefficients η_R and η_T for 1-keV incident electrons on thin Al films, and for a normal incidence, obtained with and without ionizing collisions. The backscattering yield η_R is not much modified by including the ionizing collisions, while the transmission yield η_T is much more affected. That clearly indicates that the ionizing collisions play an important role in SEE by the limitation of the penetration of the primaries into the target. Additional calculations were also made, considering only the inelastic-scattering events due to the inner shells, while the creation of electrons due to the relaxation processes was simply ignored. At 1 keV, we obtain $\delta=0.18$, i.e., a result which has to be compared to $\delta=0.61$ for a calculation including the whole role of the ionizing collisions and $\delta=0.37$ for a calculation which completely ignores them. This allows, by difference, to check the importance of the source effect. The results show that the second aspect, that is, the influence of the ionizing collisions as a source term, is not negligible.

The maximum range of incident electrons estimated by using Fitting's law⁹⁵ is $R=407$ Å for 1-keV electrons incident on polycrystalline Al targets.

When inner-shell collisions are included, a value of R between 300 and 350 Å can be estimated. Neglecting them leads to an estimation ranging between 400 and 450 Å.

More complete results have already been presented⁹⁶ where it was shown that the reduced coefficient $\eta_T(d/R)$ was also in good agreement with that given by Fitting⁹⁵ for Al, when ionizing collisions were included.

D. Comparisons to experiments

In Fig. 12, we compare values for δ and η calculated with our standard model (using PWEM from Smrcka's

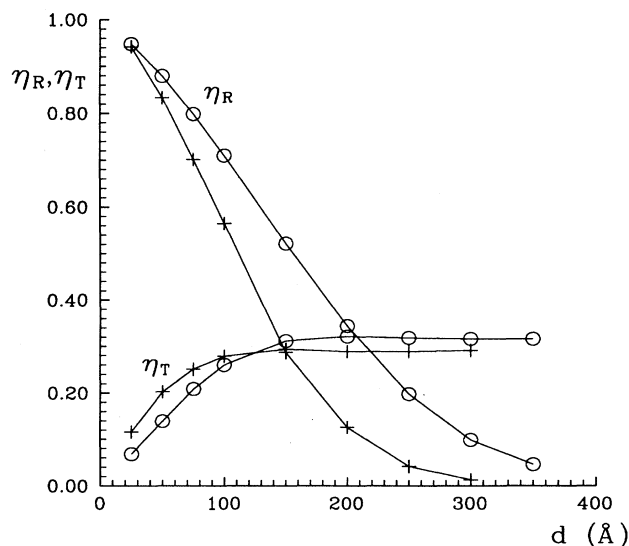


FIG. 11. Influence of the ionizing collisions. η_R and η_T backscattering coefficients as a function of the target thickness d calculated with (+) and without (o) ionizing collisions.

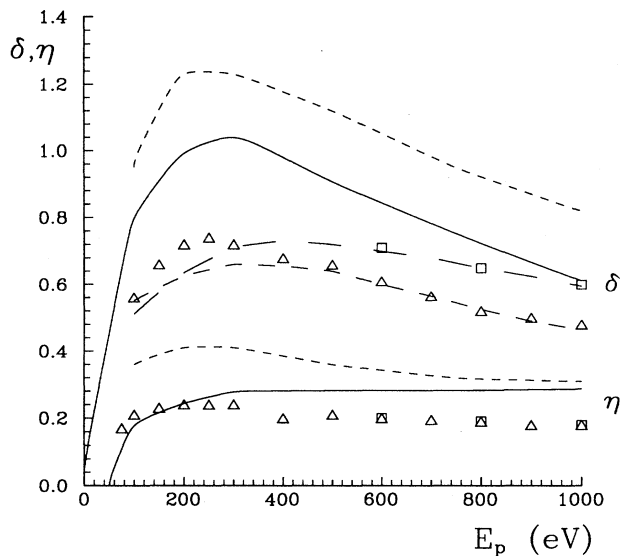


FIG. 12. Comparison of the calculated yields δ and η to experiments. The solid curves correspond to the theoretical values calculated within the standard model. The other curves correspond to experiments. The Δ 's correspond to Roptin's measurements (Ref. 97), short dashed curves correspond to Roptin's measurements corrected for the acceptance angle, the \square 's correspond to Richard's measurements (Ref. 98), medium dashed curves correspond to Bronshtein-Frajman measurements (Ref. 99) and long dashed curves correspond to Thomas-Pattinson measurements (Ref. 100).

potential,²⁵ Lindhard's function,²⁶ and Gryzinski's formula²⁷ as ingredients) to experimental results. It is clear that, at least, the order of magnitude of the calculated yields is in good agreement with experiments.

The values we have calculated for δ seem to be somewhat larger than the experimental results coming from various references.⁹⁷⁻¹⁰⁰ Let us remark that, for instance, Roptin⁹⁷ measured δ and η with an analyzer which had an acceptance angle θ_c limited to 50° . We have tried in Fig. 12 to correct the values given by Roptin for these effects. This was done by assuming a

cosinusoidal distribution for the emitted electrons. In that case, the correction simply amounts in multiplying the above results by a factor $1/\sin^2\theta_c$. As a consequence, our theoretical results become bracketed between both uncorrected and corrected results.

V. CONCLUSION

One aim of this paper has been to recall the diversity of the assumptions made by various authors working on SEE in their theoretical models.

Our own study based on a Monte Carlo simulation model has led stress on the influence of these assumptions on the SE calculated yields for 100 eV–1 keV primary electrons incident normally on polycrystalline Al targets.

First, we have emphasized the effect of the elastic collisions which limit the penetration of the primary electrons into the target and also make the internal excited SE flux more isotropic. Second, we have tested the influence of the choice of the dielectric function used to describe the excitations of the conduction electrons. Stress has been led on the MFP values issuing from these various functions. More differential aspects have been ignored. Last, the role of the ionizing collisions was considered. These are responsible for an additional source term and also they limit appreciably the penetration of the primary beam. All these modifications give appreciable differences in the computed yields.

A comparison between theoretical estimations and experiments shows that the correct order of magnitude is gained in our model. However, it is quite evidently rather difficult to extract from the experimental measurements the precise role of such and such theoretical ingredient. This also makes sometimes imprecise a complete comparison between various models.

ACKNOWLEDGMENTS

A. Dubus is grateful for financial support from Fonds National de la Recherche Scientifique (Belgium).

¹R. Bindi, H. Lantéri, and P. Rostaing, *Scanning Microsc.* **1**, 1475 (1987).

²J. Schou, *Scanning Microsc.* **2**, 607 (1988).

³A. Dubus, J. Devooght, and J.-C. Dehaes, *Scanning Microsc.* **4**, 1 (1990).

⁴M. Cailler and J.-P. Ganachaud, in *Fundamental Electron and Ion Beam Interactions with Solids for Microscopy, Microanalysis and Microlithography, Scanning Microscopy Supplement 4*, edited by J. Schou, P. Kruit, and D. Newbury (Scanning Microscopy International, AMF O'Hare, 1990), pp. 57–79.

⁵M. Cailler and J.-P. Ganachaud, in *Fundamental Electron and Ion Beam Interactions with Solids for Microscopy, Microanalysis and Microlithography, Scanning Microscopy Supplement 4* (Ref. 4), pp. 81–110.

⁶M. Rösler and W. Brauer, in *Particle Induced Electron Emission I*, edited by G. Höhler (Springer-Verlag, Berlin, 1991), pp. 1–65.

⁷J. Devooght, J.-C. Dehaes, A. Dubus, M. Cailler, and J.-P. Ganachaud, in *Particle Induced Electron Emission I* (Ref. 6), pp. 67–128.

⁸H. Bruining, *Physics and Applications of Secondary Electron Emission* (Pergamon, London, 1954).

⁹E. M. Baroody, *Phys. Rev.* **78**, 780 (1950).

¹⁰P. A. Wolff, *Phys. Rev.* **95**, 56 (1954).

¹¹E. J. Sternglass, *Phys. Rev.* **108**, 1 (1957).

¹²H. W. Streitwolf, *Ann. Phys. (Leipzig)* **7**(3), 183 (1959).

¹³H. Stolz, *Ann. Phys. (Leipzig)* **7**(3), 197 (1959).

¹⁴A. J. Bennett and L. M. Roth, *Phys. Rev. B* **5**, 4309 (1972).

¹⁵M. S. Chung and T. E. Everhart, *Phys. Rev. B* **15**, 4699 (1977).

- 16J. Schou, *Phys. Rev. B* **22**, 2141 (1980).
- 17H. A. Bethe, M. E. Rose, and L. P. Smith, *Proc. Am. Philos. Soc.* **78**, 573 (1938).
- 18C. N. Berglund and W. E. Spicer, *Phys. Rev.* **136**, A1030 (1964).
- 19M. Cailler, thèse d'Etat de l'Université de Nantes, 1969.
- 20J.-P. Ganachaud, thèse d'Etat de l'Université de Nantes, 1977.
- 21M. Cailler and J.-P. Ganachaud, *J. Microsc. Spectrosc. Electron.* **5**, 415 (1980).
- 22J.-P. Ganachaud and M. Cailler, *Surf. Sci.* **83**, 498 (1979).
- 23J.-P. Ganachaud and M. Cailler, *Surf. Sci.* **83**, 519 (1979).
- 24L. I. Schiff, *Quantum Mechanics* (McGraw-Hill, New York, 1955).
- 25L. Smrcka, *Czech. J. Phys. B* **20**, 291 (1970).
- 26J. Lindhard, *Mat. Fys. Medd. Dan. Vid. Selsk.* **28**(8), 1 (1954).
- 27M. Gryzinski, *Phys. Rev.* **138**, A305 (1965); **138**, A322 (1965); **138**, A336 (1965).
- 28J. Pillon *et al.*, in *Proceedings of the 7th International Vacuum Congress and 3rd International Conference on Solid Surfaces*, Vienna, 1977 (IUVSTA, Vienna, 1977), pp. 473–476.
- 29J.-P. Ganachaud and M. Cailler, in *Proceedings of the Second Colloque International de Physique et Chimie des Surfaces*, Brest, 1975 (SFV, Paris, 1975), pp. 3–7.
- 30H. Mignot, thèse de troisième cycle de l'Université de Nantes, 1974.
- 31K. Barzine, thèse de troisième cycle de l'Université de Nantes, 1983.
- 32M. Cailler and J.-P. Ganachaud, *Surf. Sci.* **154**, 524 (1985).
- 33M. Cailler, K. Barzine, and J.-P. Ganachaud, *Surf. Sci.* **154**, 548 (1985).
- 34M. Cailler, K. Barzine, D. Roptin, and J.-P. Ganachaud, *Surf. Sci.* **154**, 575 (1985).
- 35T. Koshikawa and R. Shimizu, *J. Phys. D* **7**, 1303 (1974).
- 36R. Shimizu, Y. Kataoka, T. Ikuta, T. Koshikawa, and H. Hashimoto, *J. Phys. D* **9**, 101 (1976).
- 37S. Ichimura, M. Aratama, and R. Shimizu, *J. Appl. Phys.* **51**, 2853 (1980).
- 38R. Shimizu and S. Ichimura (unpublished).
- 39S. Ichimura and R. Shimizu, *Surf. Sci.* **112**, 386 (1981).
- 40S. Ichimura, R. Shimizu, and T. Ikuta, *Surf. Sci.* **115**, 259 (1982).
- 41S. Ichimura, R. Shimizu, and J.-P. Langeron, *Surf. Sci.* **124**, L49 (1983).
- 42Z. J. Ding and R. Shimizu, *Surf. Sci.* **197**, 539 (1988).
- 43R. A. Bonham and T. G. Strand, *J. Chem. Phys.* **39**, 2200 (1963).
- 44T. G. Strand and R. A. Bonham, *J. Chem. Phys.* **40**, 1686 (1964).
- 45E. R. Krefting and L. Reimer, in *Quantitative Analysis with Electron Microprobes and Secondary Ion Mass Spectrometry*, edited by E. Preuss (Zentralbibliothek der KFA, Jülich, GmbH, 1973), pp. 114–148.
- 46P. Rostaing, R. Bindi, H. Lantéri, and P. Keller, *J. Phys. D* **10**, 1991 (1977).
- 47P. Rostaing, thèse de spécialité de l'Université de Nice, 1977.
- 48H. Lantéri, R. Bindi, and P. Rostaing, *J. Phys. D* **13**, 677 (1980).
- 49H. Lantéri, R. Bindi, and P. Rostaing, *Vide* **196**, 79 (1979).
- 50R. Bindi, H. Lantéri, and P. Rostaing, *J. Phys. D* **13**, 267 (1980).
- 51M. Cailler and J.-P. Ganachaud, *J. Phys. (Paris)* **33**, 903 (1972).
- 52C. Wehenkel, *J. Phys. (Paris)* **36**, 199 (1975).
- 53P. Rostaing, R. Bindi, and H. Lantéri, *Thin Solid Films* **135**, 277 (1986).
- 54H. Lantéri, P. Rostaing, and R. Bindi, *Thin Solid Films* **135**, 289 (1986).
- 55N. D. Mermin, *Phys. Rev. B* **1**, 2362 (1970).
- 56M. Rösler and W. Brauer, *Phys. Status Solidi B* **104**, 161 (1981).
- 57M. Rösler and W. Brauer, *Phys. Status Solidi B* **104**, 575 (1981).
- 58C. Kittel, *Quantum Theory of Solids* (Wiley, New York, 1963).
- 59N. W. Ashcroft, *Phys. Lett.* **23**, 48 (1966).
- 60A. O. E. Animalu and V. Heine, *Philos. Mag.* **12**, 1249 (1965).
- 61M. Rösler and W. Brauer, *Phys. Status Solidi B* **126**, 629 (1984).
- 62W. Brauer and M. Rösler, *Phys. Status Solidi B* **131**, 177 (1985).
- 63M. Rösler, *Theorie der Sekundärelektronenemission und ioneninduzierten kinetischen Elektronenemission einfacher Metalle* (Habilitationsschrift, Berlin, 1987).
- 64M. Rösler and W. Brauer, *Phys. Status Solidi B* **148**, 213 (1988).
- 65J. B. Pendry, *Low Energy Electron Diffraction* (Academic, London, 1974).
- 66M. Rösler and W. Brauer, *Phys. Status Solidi B* **156**, K85 (1989).
- 67M. Rösler and W. Brauer, *Nucl. Instrum. Methods B* **67**, 641 (1992).
- 68A. Dubus, thèse de doctorat de l'Université Libre de Bruxelles, 1987.
- 69J. Devooght, A. Dubus, and J.-C. Dehaes, *Phys. Rev. B* **36**, 5093 (1987).
- 70A. Dubus, J. Devooght, and J.-C. Dehaes, *Phys. Rev. B* **36**, 5110 (1987).
- 71M. M. R. Williams, *The Slowing-Down and Thermalization of Neutrons* (North-Holland, Amsterdam, 1966).
- 72A. Dubus, J. Devooght, and J.-C. Dehaes, *Nucl. Instrum. Methods B* **13**, 623 (1986).
- 73J. Devooght, A. Dubus, and J. Dehaes, in *International Topical Meeting on Advances in Reactor Physics, Mathematics and Computation*, Paris, 1987 (CEC and OECD/NEA, Paris, 1987), pp. 339–349.
- 74S. Chandrasekhar, *Radiative Transfer* (Dover, New York, 1960).
- 75J. Devooght, A. Dubus, and J.-C. Dehaes, *Nucl. Instrum. Methods B* **67**, 650 (1992).
- 76A. Jablonski, *Surf. Interface Anal.* **14**, 659 (1989).
- 77E. Bauer, *J. Vac. Sci. Technol.* **7**, 3 (1970).
- 78E. Bauer, in *Interactions on Metal Surfaces*, edited by R. Gomer (Springer-Verlag, Berlin, 1975), pp. 225–274.
- 79T. L. Loucks, *Augmented Plane Wave Method. A Guide to Performing Electronic Structure Calculations* (Benjamin, New York, 1967).
- 80G. Wentzel, *Z. Phys.* **40**, 590 (1927).
- 81D. Pines, *Elementary Excitations in Solids* (Benjamin, New York, 1963).
- 82A. A. Kugler, *J. Stat. Phys.* **12**, 35 (1975).
- 83G. D. Mahan, *Many-Particle Physics* (Plenum, New York, 1990).
- 84P. Vashishta and K. S. Singwi, *Phys. Rev. B* **6**, 875 (1972).
- 85F. Brosens, L. F. Lemmens, and J. T. Devreese, *Phys. Status Solidi B* **74**, 45 (1976).
- 86F. Brosens, J. T. Devreese, and L. F. Lemmens, *Phys. Status Solidi B* **80**, 99 (1977).
- 87P. Zacharias, *J. Phys. C* **7**, L26 (1974).
- 88P. Zacharias, *J. Phys. F* **5**, 645 (1975).

- ⁸⁹C. J. Tung and R. H. Ritchie, *Phys. Rev. B* **16**, 4302 (1977).
- ⁹⁰M. Hasegawa, *J. Phys. Soc. Jpn.* **31**, 649 (1971).
- ⁹¹H. Raether, *Surface Plasmons on Smooth and Rough Surfaces and on Gratings* (Springer-Verlag, Berlin, 1988).
- ⁹²P. J. Feibelman, *Surf. Sci.* **36**, 558 (1973).
- ⁹³J.-P. Ganachaud, M. Cailler, D. Aberdam, E. Blanc, and C. Gaubert, *Surf. Sci.* **87**, 129 (1979).
- ⁹⁴B. Davison, *Neutron Transport Theory* (Oxford University Press, London, 1957).
- ⁹⁵H. J. Fitting, *Phys. Status Solidi A* **26**, 525 (1974).
- ⁹⁶C. Dejardin-Horgues, J.-P. Ganachaud, and M. Cailler, *J. Phys. C* **9**, L633 (1976).
- ⁹⁷D. Roptin, thèse de docteur-ingénieur de l'Université de Nantes, 1975.
- ⁹⁸C. Richard, thèse de spécialité de l'Université de Provence, 1974.
- ⁹⁹I. M. Bronshtein and B. S. Frajman, *Secondary Electron Emission* (in Russian) (Naouka, Moscow, 1969).
- ¹⁰⁰S. Thomas and E. B. Pattinson, *J. Phys. D* **3**, 349 (1970).